

Dispersion of passive tracers in a confined convective flow

Stefania Espa^{a,*}, G. Querzoli^b, A. Cenedese^a

^a *Dipartimento di Idraulica Trasporti e Strade, Università di Roma 'La Sapienza' Via Eudossiana 18, 00184, Roma, Italy*

^b *Dipartimento di Ingegneria del Territorio, Università di Cagliari P.zza d'Armi 1, 90123, Cagliari, Italy*

(Received 21 January 2000; accepted 6 December 2000)

Abstract – A confined convective flow is experimentally studied at different Rayleigh numbers. Particle Tracking Velocimetry (PTV) technique is used both to reconstruct Lagrangian trajectories and to evaluate Eulerian flow field. Dispersion properties of the flow are investigated by means of Lagrangian statistics on particle displacements. For each run of the experiment, single particle statistics have been evaluated both on the whole set of trajectories and by selecting trajectories starting in phase from different region of the flow domain. These regions are identified according to the local geometrical characteristics of the velocity field. © 2001 Éditions scientifiques et médicales Elsevier SAS

confined convective flow / Lagrangian statistics

1. Introduction

The understanding of transport and mixing properties of passive tracers in fluid flows, having remarkable implications in several fields of earth-sciences and engineering [1], is of particular concern both in theoretical and in applied research. Ideas related to dynamical system theory, have been recently applied to the study of transport and mixing phenomena [2] in order to define suitable tools for characterizing and quantifying dispersion. This approach, has revealed particularly useful when the applicability of classical diffusion theory does not give any relevant information about the spreading mechanisms, i.e. in evaluating asymptotic mixing properties of the flow when the characteristic length scale of the velocity field is of the same order of the dimension domain [3].

The most natural approach for investigating passive scalar dynamics is a Lagrangian view in which particles result advected by a given Eulerian velocity field $\mathbf{u}(\mathbf{x}, t)$ according to the differential equation:

$$\frac{d\mathbf{x}}{dt} = \mathbf{u}(\mathbf{x}, t). \quad (1)$$

In a dynamical system framework, the Lagrangian equations of motion (1) for a two-dimensional incompressible flow formally constitute an one degree of freedom Hamiltonian system with the stream function playing the role of the Hamiltonian. When the Hamiltonian is time dependant, some of the solution to (1) are expected to be chaotic. As a consequence, even simple Eulerian flows may generate unpredictable Lagrangian motion (i.e. particle trajectories show sensitivity to initial conditions) practically indistinguishable from those obtained in a complex turbulent flow [4].

* Correspondence and reprints.

E-mail address: stefania.espa@uniroma1.it (S. Espa).

On the other hand, it is possible to show the existence of a Lagrangian regular behavior of particles (i.e. two nearby trajectories do not separate exponentially in time) in a chaotic, turbulent-like velocity field. A similar situation holds in the interior of the coherent structures and is supported by numerical and experimental observation [5]. Vortices, in fact, act as impermeable barriers to particle exchange between the inside and outside of the vortex core enhancing transport of material properties trapped in their cores [6]. This phenomenon is thus of particular importance when global transport processes of material properties in geophysical flows are studied. Moreover, the described mechanism of entrainment of passive tracers into such structures for time longer than the temporal scales of the flow, determines phenomena of anomalous dispersion [7] characterized by a time dependence of the mean square displacements as $\langle \mathbf{x}^2(t) \rangle \sim t^{\nu}$ with $\nu \neq 1$.

Convective flows, represent a good model system for the investigation of transport properties since different flow regimes ranging from time-independent, spatially periodic flow up to turbulent flows can occur by changing Rayleigh number. As a consequence, transport rates vary over a wide range [8]: when the fluid is motionless, the transport is due to molecular diffusion; in the turbulent regime transport is due to advection by the flow. Time-independent and a time-periodic regime can hold between these extremes. In the time-independent regime, large-scale transport is limited by molecular diffusion between adjacent rolls while in the time-periodic regime transport is dominated by advection of particles across their boundaries. In this paper, we present an experimental study of this phenomenon; in particular, the behavior of a thermal plume induced above a linear heat source inside a rectangular vessel has been analyzed.

In these conditions, the buoyancy originates a quasi two-dimensional flow characterized by two counter-rotating vortices separated from an ascending plume that, beyond a certain value of the control parameter (i.e. the Rayleigh number Ra), starts to oscillate in a plane perpendicular to the heat source. The dimension of such structures, is of the order of magnitude of the half of the length of the vessel. The symmetry of the flow field is broken by the formation of smaller structures, that alternatively determine an oscillation of the upward current in the right and left half-field of the fluid domain. Such configuration remains unchanged in a wide range of Ra , allowing the study of the dependence of Eulerian and Lagrangian quantities on it.

Lagrangian description of the fluid motion is obtained by means of PTV technique. The characteristics of regularity, two-dimensionality and symmetry of the analyzed flow, allow a great number of particles to be tracked for a time interval greater than the characteristic time-scales of the flow.

Eulerian instantaneous velocity fields can be obtained too. As a result one takes a spatial description of the velocity field with a frequency higher than the characteristic time scales of the investigated phenomenon.

Vortical regions have been discerned from strain-rate dominated regions by analyzing the velocity gradient tensor in particular distinguishing zones characterized by complex eigenvalues from zones characterized by real eigenvalues. As a result, one gains a topological description of the flow field in terms of its local stability/instability properties.

The eduction of different topology-like points, allows to carry out a phase sampling conditioned to these different events and to characterize the structures correlated to the various configurations assumed by the velocity field as a consequence of the oscillations of the plume. Our aim is to define the role played by these structures in transport and dispersion phenomena.

The paper is organized as follows. Section 2 describes the experimental set-up and the measuring technique. In section 3 we summarize the analysis of the local topology of a flow field and the application of topological concepts to vortex structure identification. In section 4 these concepts are used to characterize the analyzed convective flow. Section 5 is devoted to a qualitative-quantitative analysis of passive tracers dispersion. Finally, section 6 contains the concluding remarks and some comments on the applicability of the methodologies here proposed in problems of geophysical concerns.

2. Experimental set-up and measuring technique

The experimental set-up consists of a rectangular tank filled with water. Horizontal dimensions of the tank are $L = 15.0 \text{ cm} \times D = 10.4 \text{ cm}$ and its vertical dimension is $H = 6 \text{ cm}$. *Figure 1* shows the vessel and the optical configuration utilized in this experiment. The upper and lower surfaces are 0.8 cm aluminum plates kept at constant temperature by means of two counter-flow heat exchangers consisting of square-shaped pipes where water flows at constant temperature.

The side walls of the tank are made of 1 cm thick perspex plates and can be considered adiabatic. The convection is generated by a linear heat source 0.8 cm in diameter placed 0.4 cm above the bottom surface of the tank in correspondence of the center line of it. The cylinder is heated by an internal electrical resistance connected to a stabilized power supply that provides the heat flux to the system with a precision of 2%. The choice of positioning the heating element out of the bottom surface [9], reveals in a reduction in heat loss due to conduction phenomena and allows a better control of the heat flux supplied to the system.

In this configuration, the system is controlled by three non-dimensional parameters: Rayleigh number, Prandtl number and aspect ratio of the tank respectively:

$$Ra = \frac{\alpha \cdot g \cdot Q \cdot H^3}{\nu \cdot \kappa \cdot \lambda}; \quad Pr = \frac{\nu}{\kappa}; \quad A = \frac{L}{H},$$

where κ is the thermal diffusivity, λ the thermal conductivity, Q the linear heat flux, α the thermal expansion coefficient, g the gravity acceleration, and ν the kinematic viscosity. In these experiments, the fluid and the geometry of the tank have not been changed, as a consequence the complexity of the system increases with Ra . This parameter is varied in the range $6.87 \cdot 10^7 \div 2.17 \cdot 10^9$ by increasing the power supplied to the heat source. It has to be noted that Rayleigh number has been evaluated by considering the linear heat flux instead of the temperature increment [10]. *Table I* summarizes the values of the control parameters and of the physical

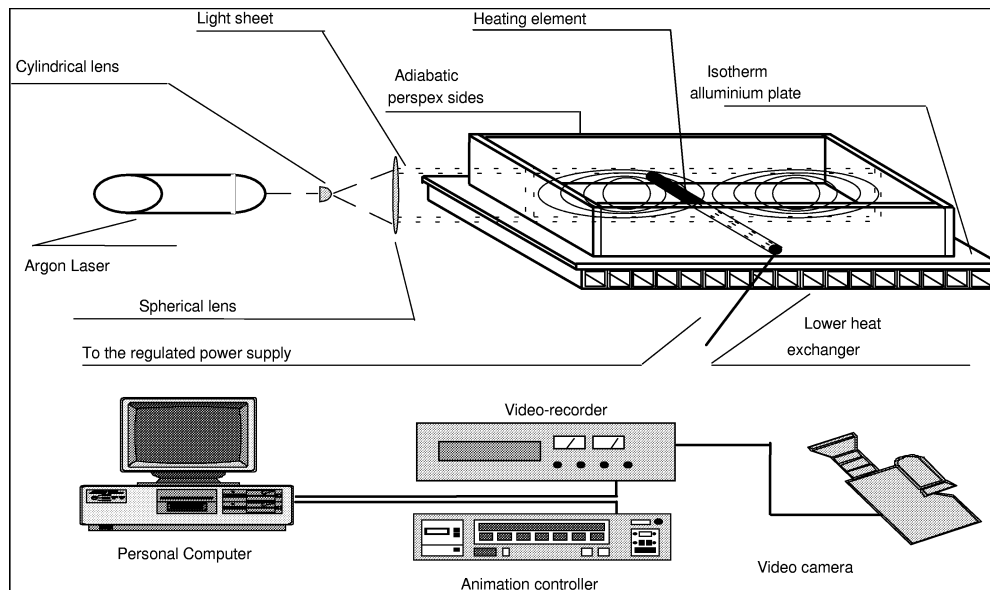


Figure 1. Experimental set-up. The upper heat exchanger (not shown) is similar to the lower one.

properties of the fluid in the different runs of the experiment. The mean temperature of the fluid, which is needed to evaluate its physical properties, is probed by a thermocouple.

PTV technique, gives the Lagrangian description of the fluid motion. Pine pollen particles of a mean size of $50 \mu\text{m}$ have been used to seed the water. The test section is a vertical plane orthogonal to the wire placed in the middle of the tank and lighted by a 0.3 cm light sheet generated by a 750 mW Argon-Ion laser beam through a cylindrical lens. Single-exposed images are acquired by a standard CCD camera placed orthogonally to the light sheet. After recording on S-VHS tape, these images are digitized at 8.33 Hz with a 752×576 pixel resolution.

A particle tracking algorithm [11], allows trajectories reconstruction by detecting positioning and tracking individual particles images over a set of the acquired frames. Velocity samples are then evaluated by dividing the particle displacements by the time interval between frames. To improve resolution, the velocities are actually evaluated using the displacements between 3 digitized frames. Eulerian velocity fields are obtained in each 4 consecutive frames by interpolating on a regular 15×35 grid.

Although PTV allows for the evaluation of velocity vectors with high local accuracy and assures a statistical independence of data, this procedure of interpolation should be carefully carried out in order to avoid errors [12].

In each run, the heat exchangers on the horizontal surfaces and the electrical resistance of the heater are activated about 3 hours before the beginning of acquisitions to avoid transient regime. Acquisitions last for 2700 s, during this period at least 22500 frames are digitized. Typically 900 particles are simultaneously

Table I. Parameters related to the analyzed runs. Q is the linear heat flux injected into the system, α the thermal expansion coefficient, ν the kinematic viscosity, κ the thermal diffusivity, λ the thermal conductivity.

Q (W/m)	α ($\text{m}^3/\text{°C}$)	ν (m^2/s)	κ (m^2/s)	λ ($\text{J}/\text{m} \cdot \text{s} \cdot \text{°C}$)	Ra	Pr
0.96×10^1	2.53×10^{-4}	8.85×10^{-7}	1.44×10^{-7}	6.031×10^{-1}	6.87×10^7	6.14
1.44×10^1	2.60×10^{-4}	8.83×10^{-7}	1.44×10^{-7}	6.03×10^{-1}	1.03×10^8	6.13
3.36×10^1	2.58×10^{-4}	8.87×10^{-7}	1.44×10^{-7}	6.02×10^{-1}	2.39×10^8	6.16
7.93×10^1	2.65×10^{-4}	8.72×10^{-7}	1.44×10^{-7}	6.04×10^{-1}	5.96×10^8	6.04
1.17×10^2	2.32×10^{-4}	9.44×10^{-7}	1.42×10^{-7}	5.98×10^{-1}	7.19×10^8	6.61
2.15×10^2	2.81×10^{-4}	8.38×10^{-7}	1.42×10^{-7}	6.067×10^{-1}	1.74×10^9	5.77
2.80×10^2	2.72×10^{-4}	8.56×10^{-7}	1.44×10^{-7}	6.053×10^{-1}	2.17×10^9	5.92

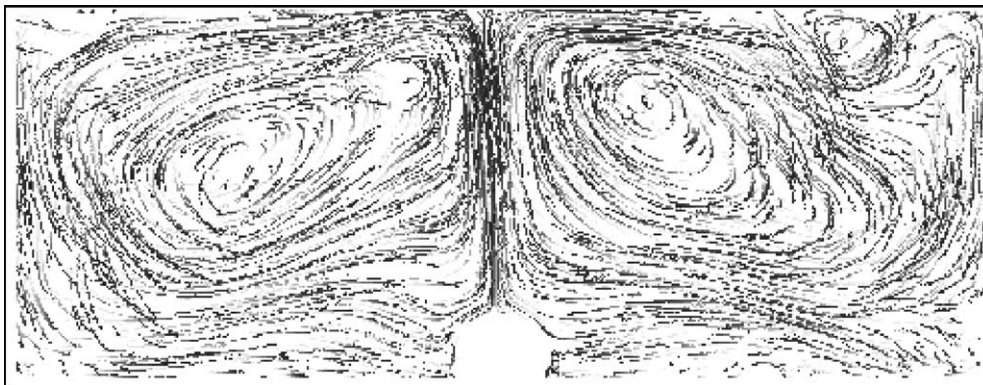


Figure 2. An example of trajectories reconstructed by PTV ($Ra = 2.39 \times 10^8$). Trajectories are followed during 100 frames of their evolution.

tracked for each frame. *Figure 2* shows an example of trajectories recognized by PTV during 100 frames of their evolution.

The scaling parameters of the flow are obtained from a non-dimensional formulation of the problem [10]. Consequently we choose as unit length the height of the cell, H , and as unit time the time scale for buoyancy effects $T = 1/N_B = (H\lambda/Qg\alpha)^{1/2}$ (N_B is the Brunt Väisälä frequency). The corresponding scale of velocity can be obtained.

2.1. Experimental observations

It has been experimentally observed that when convection starts, an ascending plume rises above the heat source and a descending flow is noted in correspondence of the side walls of the tank. This circulation organized in two counter rotating rolls divided by a buoyant plume exhibiting a natural swaying motion almost periodical

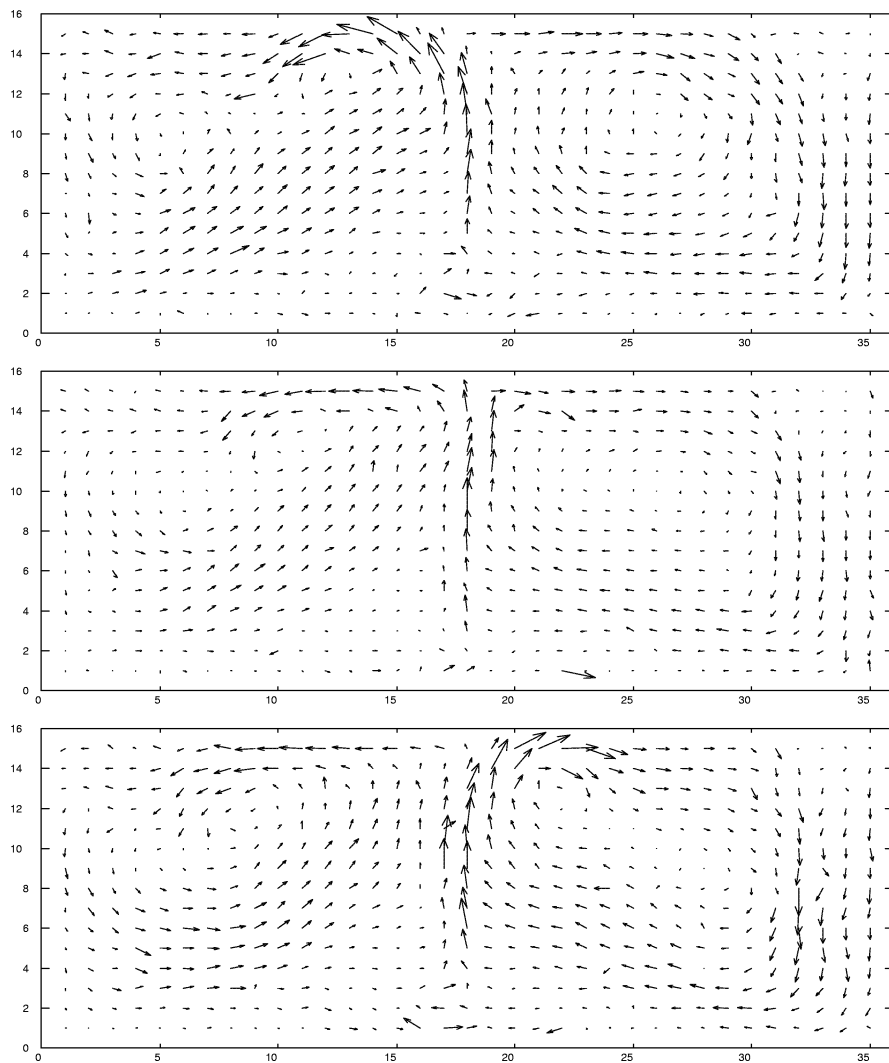


Figure 3. Swaying motion of the plume: instantaneous velocity fields ($Ra = 7.2 \cdot 10^8$).

in a plane perpendicular to the wire. No meandering instabilities in the transversal direction has been noted in the examined range of Rayleigh number.

Previous experimental and numerical evidences [9,10] have show that this flow is characterized by an alternation of different vortical structures depending on the swaying motion of the plume, i.e. on its corresponding position in the tank. In particular, two vortices form on the same side of the tank where the plume bends while, on the other side, only a structure is observes. We recover here the same flow configuration. The instantaneous velocity fields represented in *figure 3* show the oscillation of the plume at $Ra = 7.2 \cdot 10^8$.

The experimental analysis has shown the sensitivity of the system to an increasing external forcing. In particular we observe that the swaying frequency of the thermal plume depends on Rayleigh number (i.e. it increases with Ra) while the flow maintains quasi two-dimensional showing a similar pattern in the whole examined Ra range.

3. Two-dimensional analysis of the local flow topology

The relation between the Eulerian velocity field in the physical space and the dynamical system in the phase space is given by the equation of motion of the fluid particles [13]:

$$\dot{\mathbf{x}} = \mathbf{u}(\mathbf{x}, t), \quad (2)$$

where $\mathbf{x} \in X \subset \mathfrak{R}^2$ represents the position, t the evolving parameter and \mathbf{u} the velocity field depending on position and time. Considering the Taylor expansion of the non linear velocity field around a fixed point \mathbf{x}_0 , equation (2) becomes

$$\dot{\mathbf{x}} = \mathbf{u}(\mathbf{x}_0, t_0) + \mathbf{A}\mathbf{y} + o(|\mathbf{y}|^2), \quad (3)$$

where $\mathbf{y} = \mathbf{x} - \mathbf{x}_0$ is the displacement vector joining \mathbf{x} and \mathbf{x}_0 and $\mathbf{A} = \nabla \mathbf{u}$ is the velocity gradient tensor. Equation (3) can be linearized around \mathbf{x}_0 by neglecting the higher-order terms yielding to the corresponding linearized dynamical system

$$\dot{\mathbf{y}} = \mathbf{A}\mathbf{y} \quad (4)$$

which physically corresponds to the velocity field seen in a reference frame centered in \mathbf{x}_0 and moving with the velocity $\mathbf{u}(\mathbf{x}_0, t_0)$. The local geometry of the flow in the neighbor of \mathbf{x}_0 , can be investigated by analyzing the eigenvalues λ_1 and λ_2 of \mathbf{A} , i.e. by solving the eigenvalue problem:

$$(\mathbf{A} - \lambda \mathbf{I})\mathbf{e} = 0, \quad (5)$$

where e_1 and e_2 are the corresponding eigenvectors. The eigenvalues of \mathbf{A} satisfies the characteristic equation:

$$\lambda^2 - p\lambda + q = 0, \quad (6)$$

where $p = \text{trace } \mathbf{A}$, $q = \det \mathbf{A}$ are the tensor invariants. If λ_i ($i = 1, 2$) are complex, the discriminant of equation (6) $\Delta = p^2 - 4q$ is negative and the local resulting motion is rotational implying a prevalence of the anti-symmetric part of \mathbf{A} known as the rate of rotation tensor $W_{ij} = 1/2(\partial u_i / \partial x_j - \partial u_j / \partial x_i)$. On the contrary, if λ_i are real, Δ is positive and the local resulting motion is characterized by a prevalence of the symmetric part of \mathbf{A} known as the rate of strain tensor $S_{ij} = 1/2(\partial u_i / \partial x_j + \partial u_j / \partial x_i)$. A more general and detailed discussion of this topic can be found in [14].

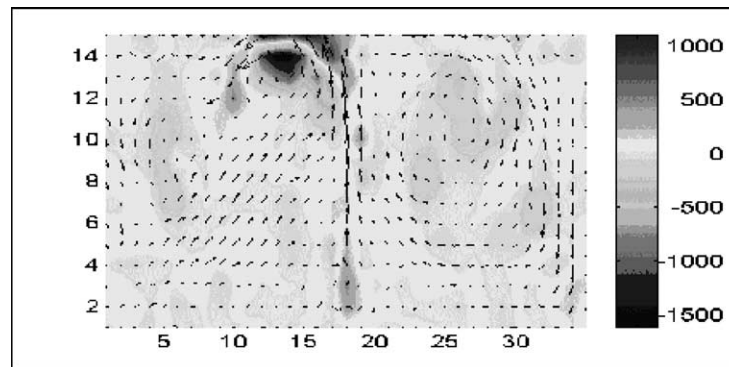
3.1. Vortex structure identification

The outlined classification of the local topology of the flow is the basis for a vortex structure identification methodology which has been used to deduce the presence of the plume in different sides of the tank.

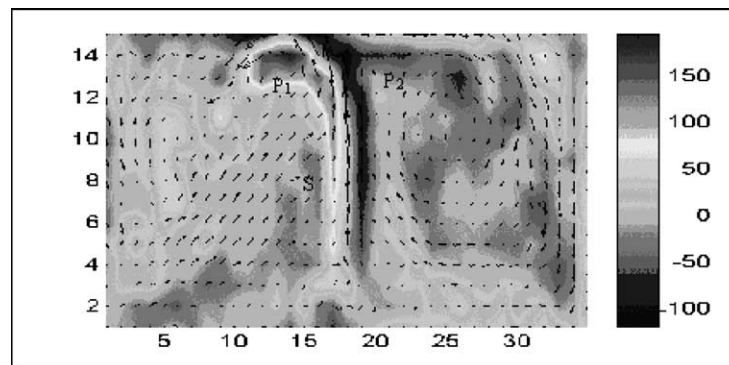
According to Desrayaud and Lauriat [10], in the examined Ra range, an intermittently chaotic state is observed. This regime is characterized by interruptions of the periodic laminar motion by non-periodic ‘bursts’ which occurs at irregular times and for irregular duration. As a result, the plume oscillates with different frequencies during the whole experiment and its position is not trivially predictable [9].

The developed method, consists in analyzing the velocity tensor gradient invariants. In previous section, it has been shown how complex eigenvalues of the velocity gradients ($\Delta < 0$) indicate particles rotation around a fixed point: this property can be used to unambiguously deduce vortical structures [14]. Let us recall that the velocity gradient tensor is reference frame invariant and consequently is independent of an observer.

Figure 4 shows the isosurfaces of the discriminant Δ (a) and of the vorticity ω (b) evaluated at $Ra = 7.2 \cdot 10^8$ for an instantaneous velocity field characterized by the presence of the plume on the left side of the tank. Using the discriminant analysis, the vortical structure existing in correspondence of the plume is clearly identified by the negative peak of Δ . Isosurfaces of vorticity, indicate a maximum in correspondence of the same structure but vorticity of the same order of magnitude is found near the separatrix S (figure 4(b)) of the flow even if no vortical structure exists. By cross sectioning the examined flow field at row 14 and plotting the distribution of



(a)



(b)

Figure 4. Isosurfaces of dimensionless discriminant (a), dimensionless vorticity (b) at the dimensionless time $t^* = 11$ ($Ra = 7.2 \cdot 10^8$).

Δ , and of ω as sketched in *figure 5*, the comparison is more evident. The negative peak of Δ is related to a positive peak in ω distribution (*A*). In *B* we observe a negative peak of (clockwise) vorticity but no structure is present ($\Delta > 0$). Let us observe that the discriminant analysis allows pure strain motion to be cut off from zones characterized by high vorticity values (*C*). Furthermore this methodology allows an objective identification of vortical structures that it is objective since no threshold on Δ is necessary.

The time histories of Δ in $P_1(13, 14)$ for the left side and $P_2(22, 14)$ for the right side (*figure 4(b)*), has then been analyzed in order to select peaks in the distributions corresponding to the vortex structure associated with the bend of the plume. As shown in *figure 6*, these peaks have been selected after normalizing the signal Δ with its standard deviation and using a threshold to filter out small fluctuations.

The analysis of these signals in the frequency domain allows to investigate the dependence of the oscillation frequency of the educed plume on Ra . The observation of the power spectrum of Δ for different Ra confirms a decreasing period and a different behavior for increasing values of the control parameter [9]. In particular, for lower values of Ra , the spectrum is characterized by a single sharp frequency while as Ra increases, the

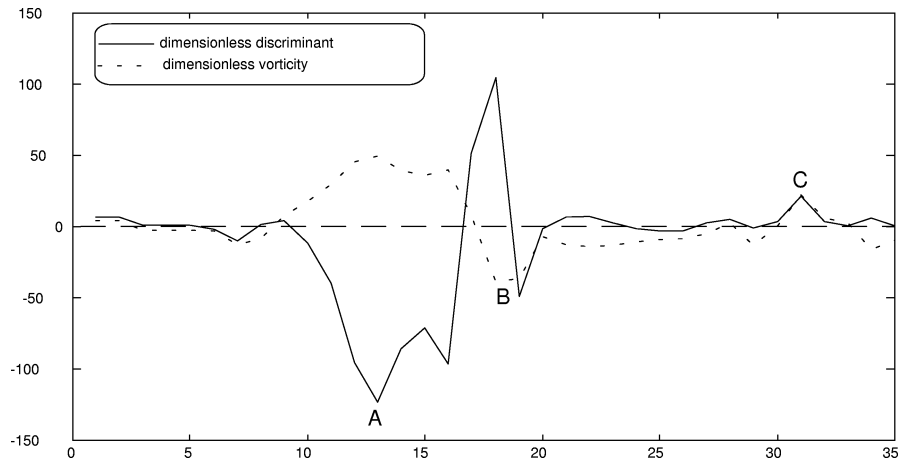


Figure 5. Cross section of the dimensionless discriminant (Δ) and of the dimensionless vorticity (ω) at row 14 of the domain ($t^* = 11, Ra = 7.2 \cdot 10^8$).

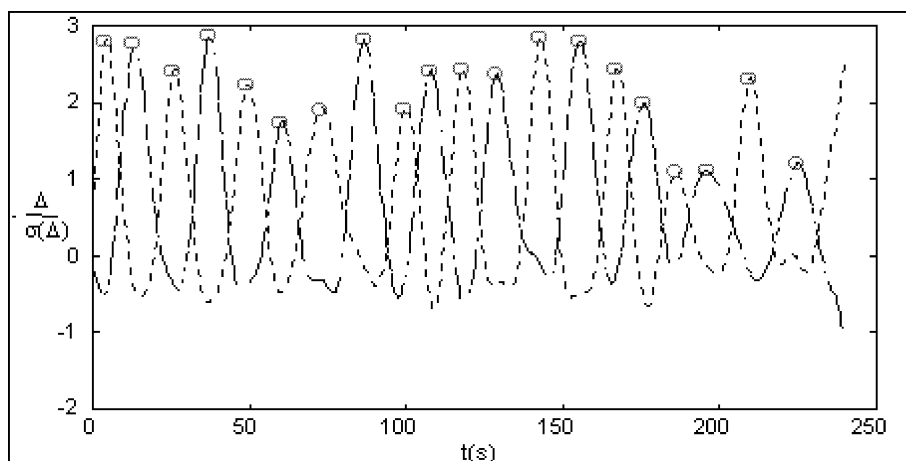


Figure 6. Time history of $(-\Delta)$ in $P_1(14, 13)$ and $P_2(14, 22)$ (*figure 5*). The peaks correspond to the vortex structure associated with the bend of the plume (--- plume on the left, — — — plume on the right).

spectrum is characterized by more than one frequency and a random alternation in time of regular-irregular oscillation is observed. In *figure 7* we plot the main dimensionless frequencies ν_* versus Ra .

A clear scaling is observed indicating a power law dependence $\nu_* \sim Ra^{0.5}$.

The extraction of the time instants corresponding to the different position of the plume in P_1 and P_2 , allows to perform a conditional sampling and to evaluate conditional averaged quantities. Conditional average is defined as an ensemble average taken over many events that satisfy a certain chosen condition [15]. The following scheme has been applied to obtain conditional average: (i) recognition of the existence of an identifiable and recurring event (negative peak in Δ distribution), (ii) selection of similar events through conditioning.

Any sampled signal $f(\mathbf{x}, t)$ can be subsequently decomposed into an ensemble-averaged part $\langle f \rangle(\mathbf{x}, t)$ and a fluctuating part $f_r(\mathbf{x}, t)$. In agreement with Hussain [16], in this way it is possible to educe coherent quantities. Thus, the phase average of structures is the coherent structure while the shifting of each instantaneous realization from the phase average represents the incoherent part of the signal. In *figure 8*, the phase averaged velocity field corresponding to the ‘plume on the left’ configuration is sketched. These features occurs symmetrically considering the phase averaged velocity fields corresponding to the educed ‘plume on the right’.

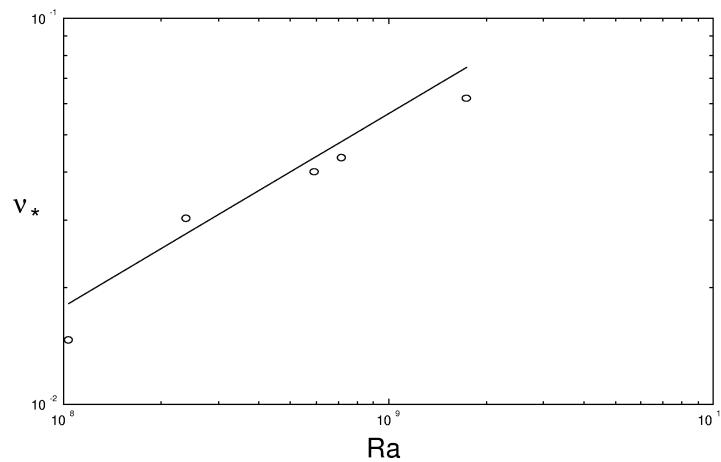


Figure 7. Main frequencies as a function of Ra . The line $Ra^{0.5}$ is also shown.

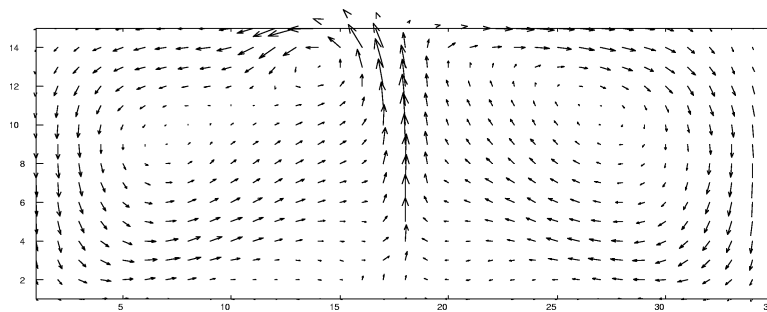


Figure 8. Phase averaged velocity field corresponding to the configuration ‘plume on the left’ ($Ra = 7.2 \cdot 10^8$).

4. Passive tracers dispersion analysis

The analysis of passive tracers dispersion inside the tank has been based on the previous considerations. As a matter of fact, from the analysis of the local topology of the instantaneous velocity field we have an indication on the local stability/instability characteristics of the flow. In order to investigate the time evolution of vortical structures during each configuration of the plume, we consider a complete oscillation of it. During the period oscillation, 5 different configuration has been considered and the corresponding instantaneous streamlines have been evaluated by integrating the velocity fields.

When the plume is on the left (*figure 9(a)*), we clearly observe two vortical structures on the same side of the plume. These structures are aligned along the diagonal of the half-field and are separated by a ‘saddle point’ *A* (i.e. in *A* λ_i are real) [17]. The strongest vortical structure used to identify the presence of the plume, topologically represents a ‘stable focus’ (i.e. in *B* λ_i are complex). This implies that the flow is not strictly two-dimensional being the structure elongated in the direction orthogonal to the measuring plane. Anyway, by evaluating $p = \nabla \cdot \mathbf{u}$, we found that the out of plane component of the velocity field is not relevant in this flow since it is some order of magnitude lower than the planar components.

From the observation of the closed streamlines around *C*, we can argue that this point can be topologically considered a ‘centre’. It corresponds to a two-dimensional vortical structure. We can notice the presence of

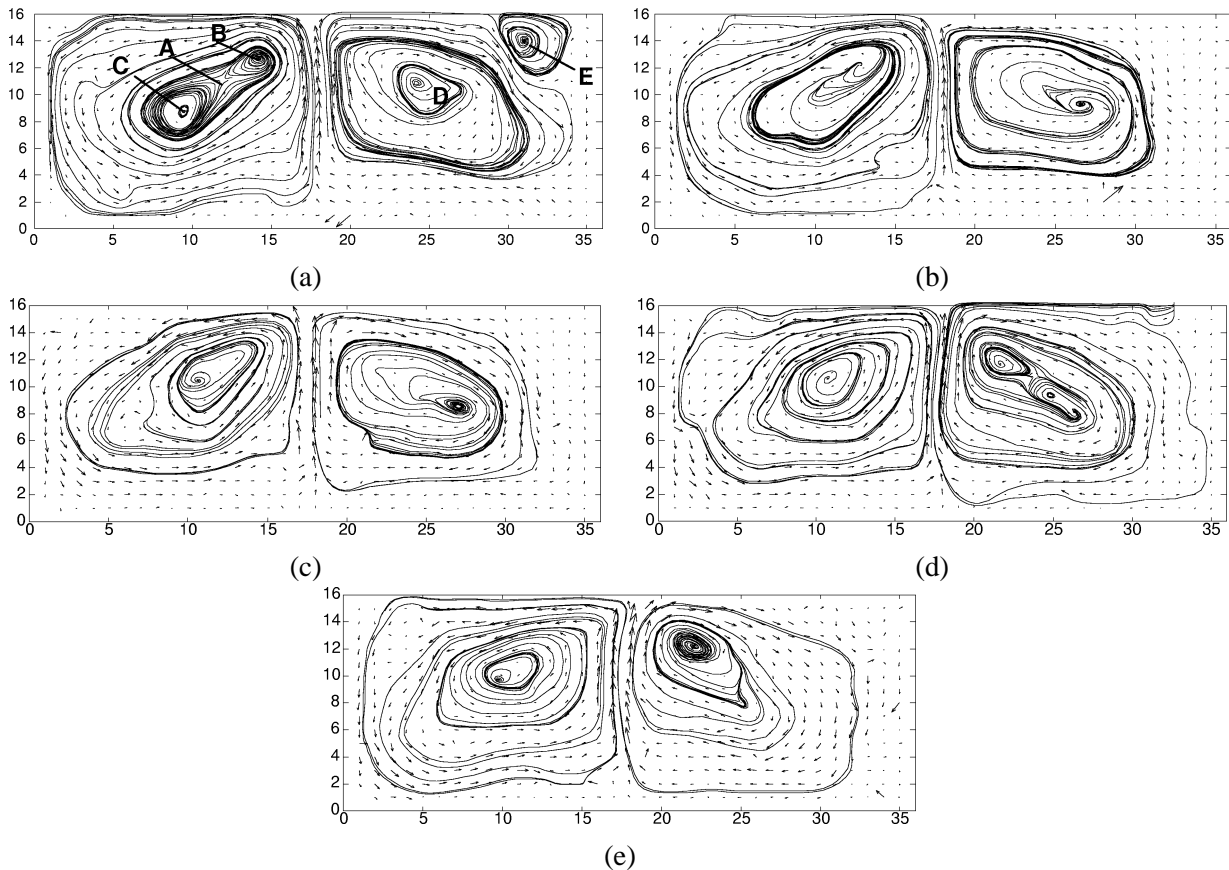


Figure 9. Instantaneous stream lines during a complete oscillation of the plume from the left (a) to the right (e) ($Ra = 7.2 \cdot 10^8$).

closed streamlines around both of these structures representing a ‘stable limit cycle’. This means that in this side of the field, mixing is instantaneously due to the presence of the saddle point *A* while the exchange of tracers between the two sides of the tank, mainly due to the oscillation of the separatrix, is weak. In the right side of the tank, a single vortical structure is present. The point *D* is a ‘stable focus’ surrounded internally by an unstable region and externally by a ‘stable limit cycle’. Mixing between these two region is limited. A re-circulating region is present in correspondence of the point *E*.

Following the evolution of the system (*figure 9(b)*), we observe the progressive merging of the two structure in the left side, while on the right side we observe an opposite phenomenon. After an oscillation period we observe a symmetric configuration when the plume is bent on the right (*figures 9(c), (d)*).

In order to obtain a qualitative description of large scale passive scalar dispersion, we place a blob of particles in correspondence of the separatrix of the flow and follow its evolution. *Figure 10* shows the evolution of the distribution of tracer particles during an oscillation. This figure shows that within the rolls the tracers are mixed very rapidly while the cross transport between the rolls is low. As a further evidence we plot in *figure 11* the trajectories of particles starting from the left or the right side. We observe that most of the particles remain confined in the convective structures while particles which effectively cross the separatrix are a small fraction of the total amount.

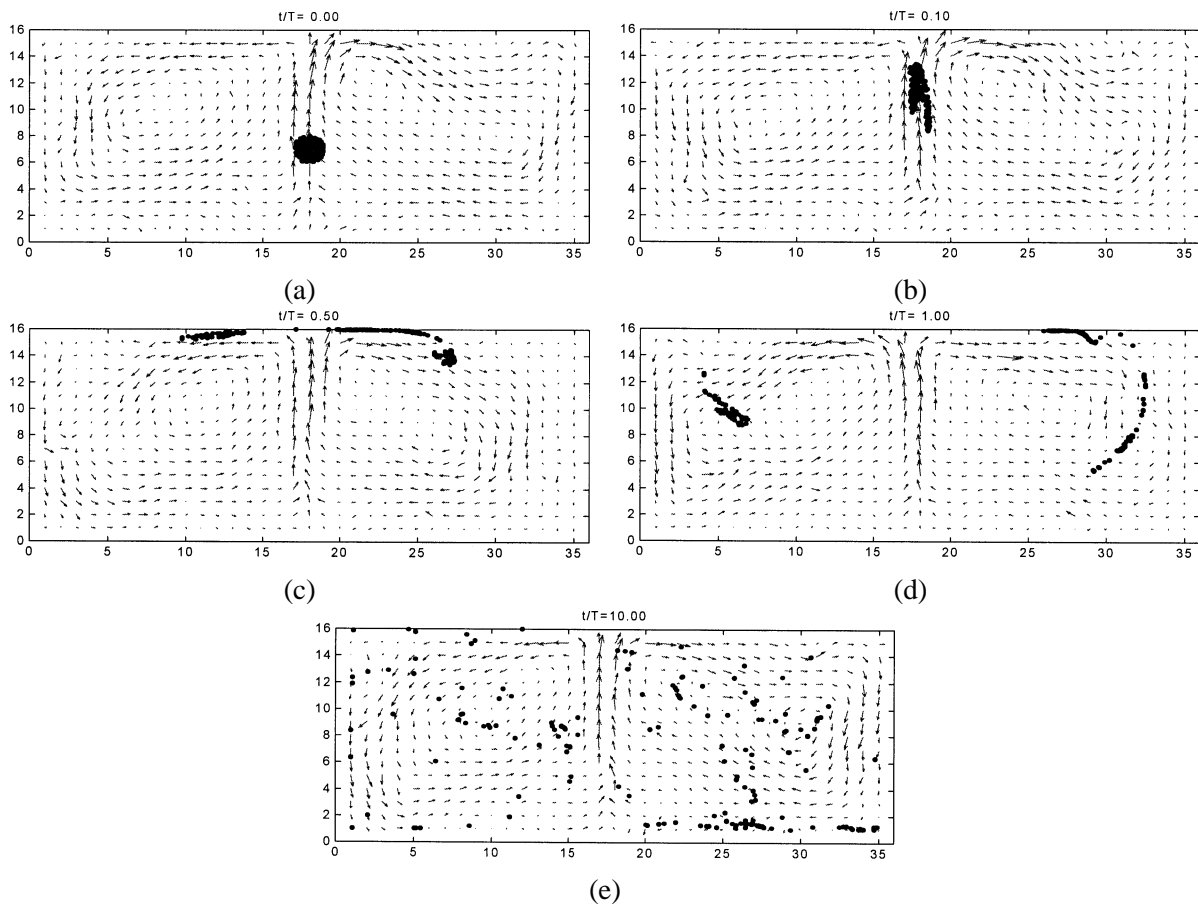


Figure 10. Large scale passive scalar dispersion ($Ra = 7.2 \cdot 10^8$).

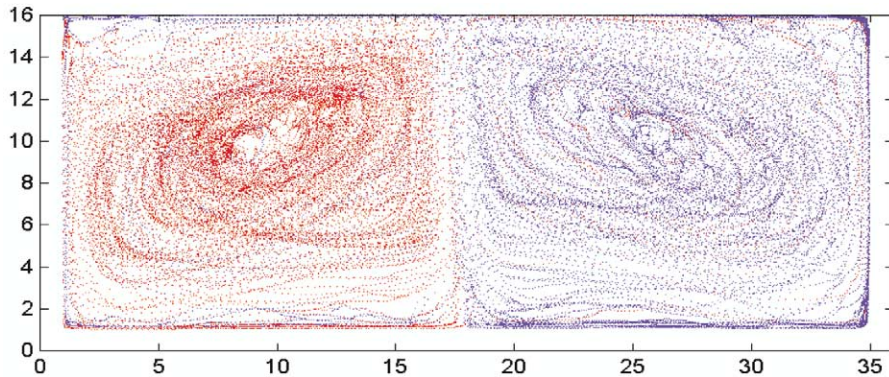


Figure 11. Cross transport between adjacent convective rolls: time evolution of tracers trajectories starting from the left side (red) and from the right side (blue).

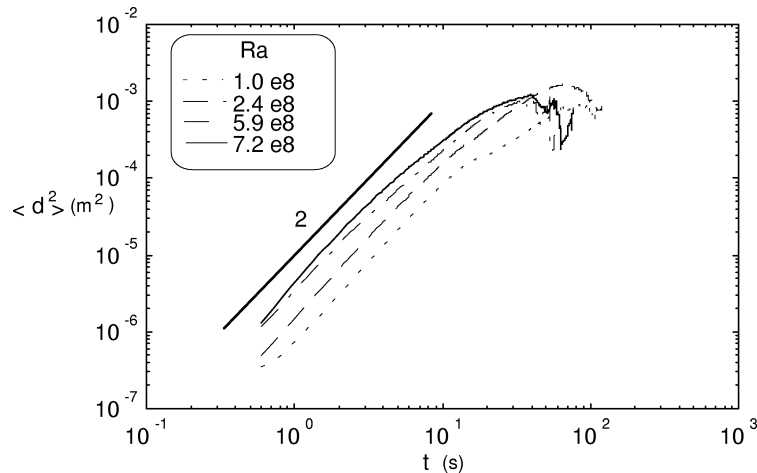


Figure 12. Mean square particles displacement versus time in log-log plot at different Ra . The line corresponding to a quadratic dependence is also shown.

In order to quantify passive tracers dispersion, we evaluate single particle statistics. In *figure 12*, the mean square particles displacement versus time is plotted for different value of Rayleigh number. As expected, dispersion increase with Ra following a parabolic law. Let us clarify that we are now quantifying dispersion by considering, for each Ra , the squared value of the displacements of all the particles in the whole domain averaged over the whole time history. This quantity gives then an indication of the mean spreading of the particles from their initial positions.

If we normalize these curves according to the introduced time and length scales a nice collapse is observed (*figure 13*). As a consequence, it is possible to educe a characteristic scale of the convective structures which is independent on Ra .

A mean residence time τ in the convective structures can be evaluated too. Considering the non-dimensional formulation of the problem, one recovers a scaling indicating a power low dependence $\tau \sim Ra^{-0.5}$ which has been previously observed for the Eulerian characteristics (see section 3.1). Characteristic time and length scales correspond to the saturation point of the curves in *figure 13*.

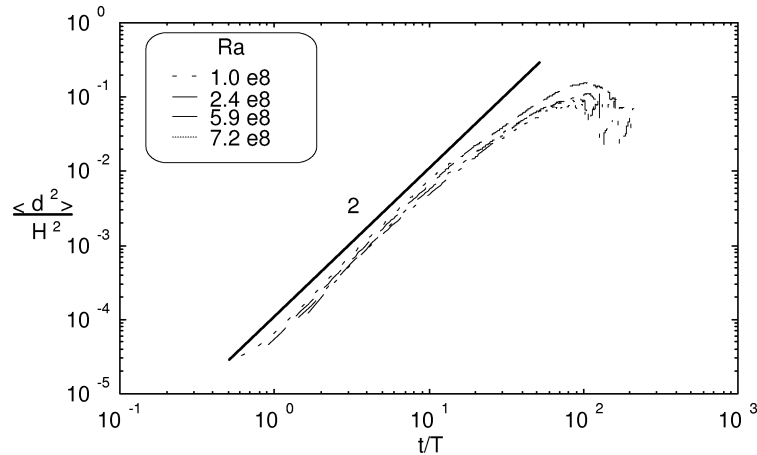


Figure 13. Dimensionless mean square particles displacement versus time in log-log plot at different Ra .

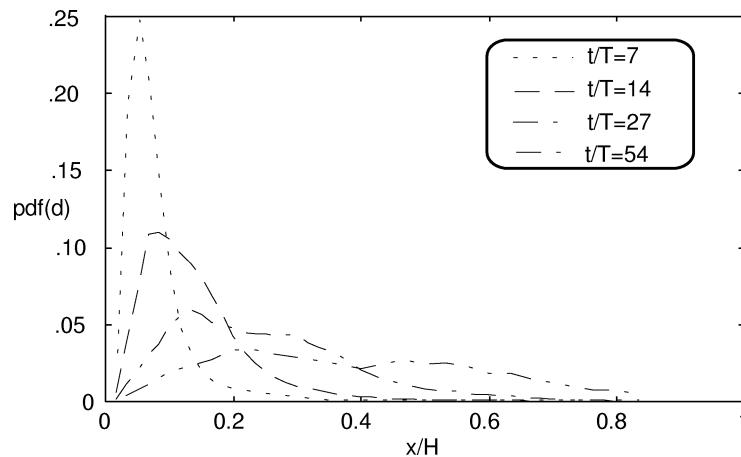


Figure 14. Probability distribution functions of displacements obtained at different time instants ($Ra = 7.2 \cdot 10^8$).

In *figure 14* we plot the probability distribution of displacements obtained at different time instants taking $Ra = \text{const} = 7.2 \cdot 10^8$. These distributions are characterized by high skewness value and by a bimodal behavior increasing as time increases. This trend can be explained by the presence of two different classes of particles characterized by different Lagrangian mean velocities indicating that there is a greater amount of particles moving away from the initial stable position as time increases.

Let us stress that the described statistics although allowing a general knowledge of dispersion phenomena, can not give a comprehensive description of it. As a matter of fact, the presence of different events and patterns correlated to the periodicity of the flow is not considered.

In order to consider the periodicity of the flow structures, we choose to identify four main regions in the flow domain, corresponding to four identified main behavior, according to the results obtained from the previous topological analysis. *Figure 15(a)* shows the selected regions considering a phase averaged flow field characterized by the plume on the left. Trajectories starting from a neighborhood of those points have been selected. A set of selected trajectories is shown given in *figure 15(b)*. The exact position of the ‘saddle point’ has not exactly selected because it lies in correspondence of the upper boundary of the domain. Using PTV to

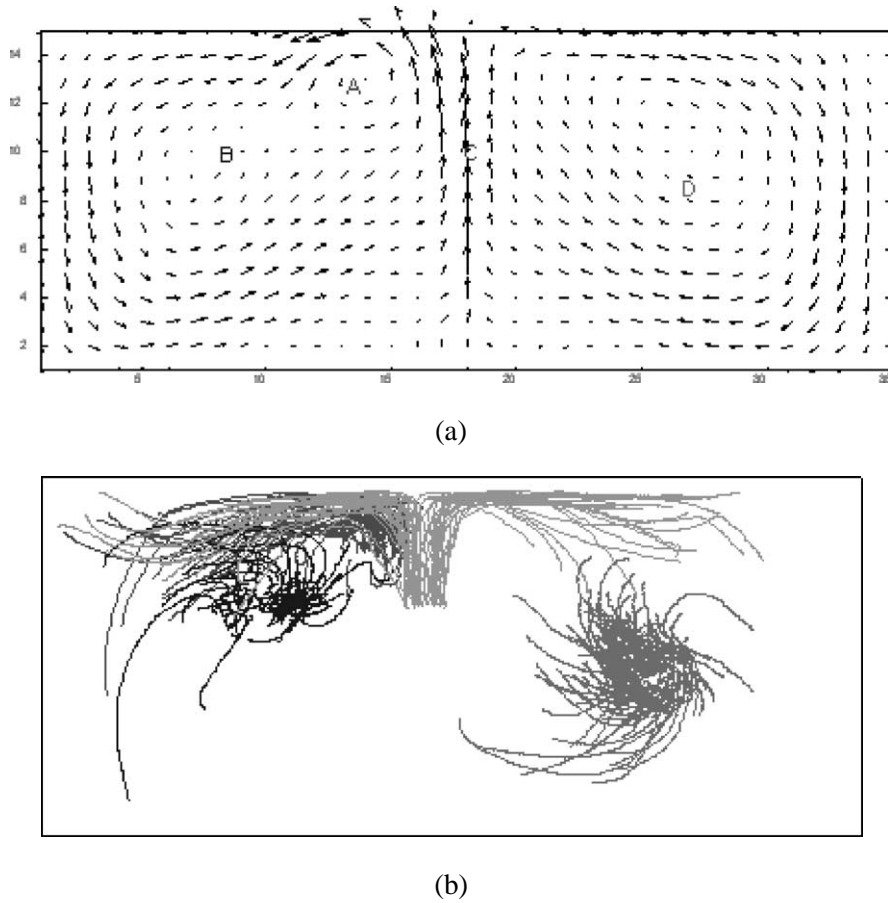


Figure 15. (a) Selection of main regions in the phase averaged velocity field corresponding to the configuration ‘plume on the left’ ($Ra = 7.2 \cdot 10^8$); (b) corresponding trajectories in phase.

measure the velocity field, trajectories can not be followed for long time intervals along the boundaries due to problems related to light reflection [11]. We consequently identify this region by selecting a point belonging to the separatrix but located below the boundary of the domain (C).

Lagrangian statistics are now evaluated on these selected samples of trajectories. In *figure 16* we plot for each identified region the mean square particles displacement versus time taking $Ra = 7.2 \cdot 10^8$. The analysis of the curves gives an evidence of the different behavior characterizing these regions. As expected, the region corresponding to the separatrix (C) is characterized by highest dispersion properties since tracers are entrained in a large scale structure. Region A is characterized by high value of dispersion too. In this region, some particles are entrained in the jet and moved away from the focal region causing highest value of the mean square displacements.

The mechanisms of dispersion depicted in this section, refer to large scale patterns contribution. The understanding of the role of the ‘chaotic advection’ mechanism [18,19] acting at the smallest scale of the flow and the corresponding evaluation of two-particles statistics, represent the further step in the investigation and in the modeling of dispersion phenomena.

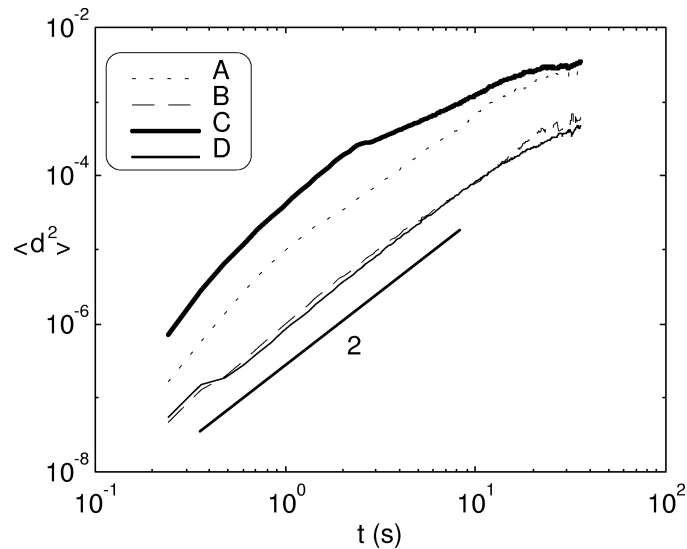


Figure 16. Mean square displacements of selected trajectories (see figure 15) versus time in log-log plot ($Ra = 7.2 \cdot 10^8$).

5. Conclusions

Transitional plumes in confined geometry are experimentally analyzed by PTV. This flow regime, is intermediate between laminar and turbulent flow. Laminar regime, occurring at small Ra , is characterized by being stationary. By increasing the forcing, the flow drives to a turbulent state. The transitional regime is characterized by being time periodic. The plume originates by an external forcing due to the heat transfer from a linear local source.

Different runs of the experiment are performed in a time periodic regime varying the heat flux supplied by the heat source and consequently the control parameter of the system Ra , which rules the complexity of the system.

PTV technique has allowed both the Lagrangian and the Eulerian description of the fluid motion and a large number of sample to evaluate statistics.

The topological analysis of the instantaneous velocity fields based on the study of the eigenvalues of the velocity gradient tensor, provides a description of the local flow geometry and a methodology for the identification of the vortical structures.

This identification method has allowed both the extraction of events correlated with the periodicity of the examined flow and a characterization of the oscillations in terms of main frequencies ν_* obtained by studying their dependence on the control parameter Ra . We find a power law dependence, i.e. $\nu_* \sim Ra^{0.5}$.

Once identified the plume in each instantaneous realization, the extraction of the time instants corresponding to two different configurations of the plume (left and right) are extracted to perform a conditional sampling and to evaluate conditional averaged quantities. As a result, it has been possible to share the velocity field in different zones characterized in mean by different behavior during a left (or a right) oscillation. This study is preliminary to the understanding of the basic mechanism which drives dispersion phenomena occurring inside the tank.

Single particle Lagrangian statistics, i.e. mean square displacement, have been performed on the whole set of reconstructed trajectories and by considering all those in the same phase and starting from the educed regions.

The results show that Lagrangian trajectories are independent on Rayleigh number resulting the Eulerian length independent on Ra . Moreover we find a power law scaling for the mean residence time in the convective structures ($\tau \sim Ra^{-0.5}$) analogous to the scaling obtained for the Eulerian characteristics (u_*). The Lagrangian statistics on selected trajectories enhance the expected different behaviour of the particles in the different educed zones.

In the analyzed convective flow we recover some of the main feature of geophysical flow: the characteristics of quasi two-dimensionality and time periodicity, the presence of coherent structures, the influence of boundaries. These analogies suggest to define a general approach in approaching the study of passive scalar dispersion in geophysical system.

Acknowledgements

We thank G.P. Romano, M. Miozzi, M. Mammetti, G. Boffetta, A. Vulpiani for useful discussions and M. Tardia for his contributions during the data acquisition. This work is partially supported by MURST (Contract N. 9908264583).

References

- [1] Moffat H.K., Transport effects associated with turbulence with particular attention to the influence of helicity, *Rep. Prog. Phys.* 46 (1983) 621.
- [2] Ottino J.M., *The Kinematics of Mixing: Stretching, Chaos and Transport*, Cambridge University Press, Cambridge, 1989.
- [3] Artale V., Boffetta G., Celani A., Cencini M., Vulpiani A., Dispersion of passive tracers in closed basins: Beyond the diffusion coefficient, *Phys. Fluids A* 9 (1997) 3162.
- [4] Crisanti A., Falcioni M., Paladin G., Vulpiani A., Lagrangian chaos: transport, mixing and diffusion in fluids, *Riv. Nuovo Cimento* 14 (1991) 1.
- [5] Provenzale A., Transport by coherent barotropic vortices, *Annu. Rev. Fluid Mech.* 31 (1999) 55.
- [6] Babiano A., Boffetta G., Provenzale A., Vulpiani A., Chaotic advection in point vortex models and two-dimensional turbulence, *Phys. Fluids* 6 (1994) 2465.
- [7] Boffetta G., Celani A., Crisanti A., Vulpiani A., Relative dispersion in fully developed turbulence: Lagrangian statistics in synthetic flows, *Europhys. Lett.* 42 (1999) 177.
- [8] Solomon T.H., Gollub J.P., Chaotic particle transport in time-dependent Rayleigh–Benard convection, *Phys. Rev. A* 38 (1998) 6280.
- [9] Miozzi M., Querzoli G., Romano G.P., The investigation of an unstable convective flow using optical methods, *Phys. Fluids* 10 (1998) 2995.
- [10] Desrayaud G., Lauriat G., Unsteady confined buoyant plumes, *J. Fluid Mech.* 252 (1993) 617.
- [11] Querzoli G., A Lagrangian study of particle dispersion in the unstable boundary layer, *Atmos. Environ.* 16 (1996) 2821.
- [12] Adrian R.J., Particle-imaging techniques for experimental fluid mechanics, *Annu. Rev. Fluid Mech.* 23 (1991) 261.
- [13] Cantwell B.J., Organized motion in turbulent flow, *Annu. Rev. Fluid Mech.* 13 (1981) 475.
- [14] Joeng G., Hussain F., On the identification of a vortex, *J. Fluid Mech.* 285 (1995) 69.
- [15] Blackwelder R.F., On the role of phase information in conditional sampling, *Phys. Fluids* 20 (1977) 232.
- [16] Hussain F., Coherent structures and turbulence, *J. Fluid Mech.* 173 (1986) 303.
- [17] Chong M.S., Perry A.E., A general classification of three-dimensional flow fields, *Phys. Fluids* 2 (1990) 765.
- [18] Boffetta G., Cencini M., Espa S., Querzoli G., Experimental evidence of Chaotic Advection in a convective flow, *Europhys. Lett.* 48 (1999) 629.
- [19] Boffetta G., Cencini M., Espa S., Querzoli G., Chaotic advection and relative dispersion in an experimental convective flow, *Phys. Fluids* 12 (2000) 1.